FAST EVALUATION OF THE BOLTZMANN COLLISION OPERATOR USING DATA DRIVEN REDUCED ORDER MODELS

ALEXANDER ALEKSEENKO, ROBERT MARTIN, AND AIHUA WOOD

ABSTRACT. We consider application of reduced order models (ROMs) to accelerating solutions of the spatially homogeneous Boltzmann equation for the class of problems of spatially homogeneous relaxation of sums of two homogeneous Gaussian densities. Approximation spaces for the ROMs are constructed by performing singular value decomposition of the solution data matrix and extracting principal singular vectors/modes. The first ROM results from a straightforward Galerkin discretization of the spatially homogeneous Boltzmann equation using a truncated basis of the singular vectors. The model approximates solutions to the Boltzmann equation accurately during early stages of evolution. However, it suffers from presence of ROM residuals at later stages and exhibits slowly growing modes for larger ROM sizes. In order to achieve stability, the second ROM evolves the difference between the solution and the steady state. The truncated singular vectors are orthogonalized to the steady state and modified locally to enforce zero density, momentum, and temperature moments. Exponential damping of ROM residuals is introduced to enforce physical accuracy of the steady state solution. Solutions obtained by the second ROM are asymptotically stable in time and provide accurate approximations to solutions of the Boltzmann equation. Complexity for both models is $O(K^3)$ where K is the number of singular vectors retained in the ROMs. For the considered class of problems, the models result in up to three orders of magnitude reduction in computational time as compared to the $O(M^2)$ nodal discontinuous Galerkin (DG) discretization, where M is the total number of velocity points.

1. Introduction

With the emergence of novel applications of rarefied gas flows in hypersonic and space flights and microscopic flows, there is an increased need for simulation tools capable of handling complex flow geometries and of accurately predicting complex physics of the flows. The Boltzmann equation is believed to be the most accurate model of rarefied gas and can provide important understanding about the applications at hand. As a result, there is a significant need to develop efficient methods for its solution. However, solution algorithms for the Boltzmann equation that would make its use practical in multiple dimension with real gas effect, proved to be difficult to obtain. A major challenge continues to be the evaluation of the multifold integral describing the effect

 $^{2000\} Mathematics\ Subject\ Classification.\ 76P05, 76M10, 65M60.$

Key words and phrases. Boltzmann kinetic equation, reduced order models, dynamics of non-continuum gas.

The first author was supported by the NSF grants DMS-1620497, DMS-2111612, and by AFOSR grant F4FGA08305J005.

The second author was supported by AFOSR grant FA955020RQCOR100.

The third author was supported by AFIT and AFOSR grant F4FGA08305J005.

The research was supported in part by the Air Force Research Laboratory Propulsion Directorate, through the Air Force Office of Scientific Research Summer Faculty Fellowship Program, Contract Numbers FA8750-15-3-6003, FA9550-15-0001 and FA9550-20-F-0005. Computer resources were provided by the Extreme Science and Engineering Discovery Environment, supported by National Science Foundation Grant No. OCI-1053575.

of molecular collisions. Development of algorithms for collision integral with low computational cost will dramatically improve applicability of the Boltzmann equation. A review of recent results can be found in [20, 48]. Straightforward discretizations of the collision operator using uniform discrete meshes in the velocity space result in $O(n^8)$ or higher complexity algorithms, where n is the number of discrete velocity points in one velocity dimension [2, 1, 8, 9, 25, 60, 42]. With the exception of the spatially homogeneous case, these discretizations become prohibitively expensive for n > 20. In [50], L. Pareschi and B. Perthame proposed a Galerkin discretization of the collision operator based on the Fourier expansion of the velocity distribution function. By exploring properties of the exponential basis, the authors derived a deterministic algorithms with $O(n^6)$ complexity and proved that the discrete collision kernel is low-dimensional. Related approaches were developed in [35, 38, 28, 24] based on applications of the Fourier transform to the collision operator. Fourier-Galerkin approaches were used to simulate gases with internal energies in [47]. Discontinuous Galerkin discretizations on uniform grids with $O(n^6)$ complexity were developed in [5].

Historically and recently, there has been a significant interest to develop algorithms of even lower computational complexity than the above examples. Development of faster methods is critical for the success of simulations of mixtures of gases and gases with internal energies. Two main directions were pursued: derivation of discretization schemes that require fewer operations than $O(n^6)$ to be used with large values of n, and methods that may have high complexity, e.g., $O(n^9)$, but that provide accurate solutions for low values of n. (The approach presented in this paper is in the second category.) A. Bobylev and S. Rjasanow developed an $O(n^4)$ algorithm for evaluating the collision integral in the case of Maxwell's pseudo-molecules in [14]. In [15], the same authors used Carleman representation of the collision operator to separate integration of the collision integral in the case of hard spheres potential reducing it to integration of onedimensional convolutions of the distribution function. The resulting approach has complexity of $O(Mn^3 \log n)$ operations. Approaches were proposed based on discrete velocity models on uniform meshes in which only small subsets of pairs of velocity points participate in evaluation of the collision integral [10, 11, 49]. In these approaches, the velocity pairs are selected so as to enforce conservation laws. An efficient method was introduced in [52] by formally applying a Galerkin discretization in the velocity variable using a basis of Dirac delta-functions defined at the nodes of a uniform velocity grid. Efficient evaluation of the collision integral is achieved by introducing quasi-stochastic Korobov integration. The method has been applied to simulation of gas mixtures and gases with internal energies in multidimensional applications [53, 39]. A related approach was developed in [43, 55] using stochastic evaluation of the multifold collision operator.

C. Mouhot and L. Pareschi [45] used Carleman representation of the collision operator and Fourier-Galerkin approximation of the velocity distribution function to develop an $O(n^3 \log n)$ approach by replacing the double integral with a sequence of decoupled one dimensional convolution integrals in the case of the hard spheres potential, see also [15, 13]. The approach was extended in [44, 22] leading to multidimensional simulations of gas in [21, 58, 36] and of gas mixtures in [59]. A generalization of the approach to discrete velocity models with uniform velocity meshes can be found in [46]. Following similar ideas, an $O(mk^4 \log k)$ algorithm was proposed in [26] for formulations based on the Fourier transform of the collision operator.

There is, however, a consensus in the research community that existing methods do not fully utilize properties of the problems yet and that more efficient methods can be proposed for evaluation of the collision operator. In [23] a hyperbolic cross approximation of the solution in the frequency space was proposed introducing adaptivity in spectral methods. A polynomial spectral discretization was proposed in [29] and applied to solution of two dimensional super sonic flows. A method based on the Fourier transform of the collision operator and using representations of the solution on non-uniform meshes was proposed in [30]. In [27] a Galerkin-Petrov discretization is proposed for the spatially homogeneous Boltzmann equation. In their approach, the velocity distribution function is approximated using products of Laguerre polynomials and spherical harmonics, allowing for compact approximations of smooth solutions. Polynomial test functions are used to make the approach conservative by construction. The methods was applied to solution of a one-dimensional Boltzmann equation in [37].

Recently, artificial neural networks and machine learning were applied to solution kinetic equations in [41]. An approach using low rank tensor approximations of model kinetic solutions was proposed in [16]. Machine learning approximation of the collision operator were developed in [32]. Among other attempts to obtain faster evaluation of the collision operator we mention [4, 3] where approximation of kinetic solutions by sums of homogeneous Gaussians was used to accelerate evaluation of the collision integral.

In this paper we use techniques of model reduction [57, 6, 7] to construct a compact discretization basis for a class of solutions to problem of spatially homogeneous relaxation. The basis is constructed by performing singular value decomposition of the collection of solutions. The reduced order model (ROM) is obtained by performing Galerkin discretization of the spatially homogeneous Boltzmann equation using the constructed basis. The complexity of the developed approach is $O(K^3)$, where K is the total number of the basis functions used in approximation. Thus the proposed approach is prohibitively expensive asymptotically. However, for the considered class of solutions, only a small number of basis functions is required achieving at least two orders of magnitude acceleration as compared to the $O(n^6)$ nodal-discontinuous Galerkin discretization [5].

2. The Reduced Order Model

2.1. **The Boltzmann equation.** In the kinetic approach the gas is described using the molecular velocity distribution function $f(t, \vec{x}, \vec{v})$ which has the property that $f(t, \vec{x}, \vec{v})d\vec{x} d\vec{v}$ represents the number of molecules that are contained in the box with the volume $d\vec{x}$ around point \vec{x} whose velocities are contained in a box of volume $d\vec{v}$ around point \vec{v} . In this work, we are concerned with the solution of the spatially homogeneous flows that correspond to the assumption that the $f(t, \vec{x}, \vec{v})$ is constant in the \vec{x} variable. In this case, the dynamics of the gas is given by the spatially homogeneous Boltzmann equation (see, for example [40, 19]),

$$\frac{\partial}{\partial t} f(t, \vec{v}) = I[f](t, \vec{v}). \tag{1}$$

Here I[f] is the molecular collision operator

$$I[f](t, \vec{v}) = \int_{\mathbb{R}^3} \int_{\mathbb{S}^2} (f(t, \vec{v}') f(t, \vec{u}') - f(t, \vec{v}) f(t, \vec{u})) B(|g|, \cos \theta) \, d\sigma \, d\vec{u}, \tag{2}$$

where \vec{v} and \vec{u} are the pre-collision velocities of a pair of particles, $\vec{g} = \vec{v} - \vec{u}$, \mathbb{S}^2 is a unit sphere in \mathbb{R}^3 centered at the origin, \vec{w} is the unit vector connecting the origin and a point on \mathbb{S}^2 , θ is the

deflection angle defined by the equation $\cos \theta = \vec{w} \cdot \vec{g}/|g|$, $d\sigma = \sin \theta \, d\theta d\varepsilon$, where ε is the azimuthal angle that parametrizes \vec{w} together with the angle θ . Vectors \vec{v}' and \vec{u}' are the post-collision velocities of a pair of particles and are computed by

$$\vec{v}' = \vec{v} - \frac{1}{2}(\vec{g} - |g|\vec{w}), \qquad \vec{u}' = \vec{v} - \frac{1}{2}(\vec{g} + |g|\vec{w}).$$
 (3)

The ROM considered in the paper is obtained by performing the standard Galerkin discretization of (1). The key difference from other approaches is that the basis functions for the discretization are obtained numerically and are closely associated with discretization [2, 5], that is used to computed it. In principle, one could consider these basis functions independently using a suitable interpolation and derive a stand alone discrete scheme. Such approach could be beneficial for spatially inhomogeneous problems, since is leads to low order discretizations of kinetic equations. Development of such discretizations will be the future authors' work. In the spatially homogeneous case, however, it appears practical to integrate the ROM with the "parental" numerical method. Specifically, the ROMs presented in this paper are implemented as subroutines in a multi-functional kinetic code and are used interchangingly with the full discretization of the collision operator as a way to accelerate computation.

2.2. Nodal-DG Discretization of the Boltzmann Equation. We will start by briefly describing the high order nodal-DG discretization in the velocity variable that is used to obtain the basis functions for the ROM. For additional detail, the reader is referred to [1, 2, 5]. We will assume that a rectangular domain in the velocity space is partitioned into uniform rectangular parallelepipeds, K_j , $j = 1, ..., M^3$, where M is the number of velocity cells in each dimension. On each element K_j of this partition we introduce a nodal-DG basis $\phi_{i;j}(\vec{v})$, $i = 1, ..., s^3$ associated with Gauss-Legendre quadrature of order s [31]. The distribution function if sought in the form

$$f(t, \vec{v}) = \sum_{\substack{i=1,s^3\\j=1,M^3}} f_{i;j}(t)\phi_{i;j}(\vec{v}).$$
(4)

Following the standard Galerkin procedure the discrete velocity form of (1) is:

$$\partial_t f_{i;j}(t, \vec{v}) = I_{\phi_{i;j}} \,, \tag{5}$$

where $I_{\phi_{i;j}}$ is the projection of the collision operator on the basis function $\phi_{i;j}(\vec{v})$:

$$I_{\phi_{i;j}} = \frac{8}{\omega_i \Delta \vec{v}} \int_{K_i} \phi_{i;j}(\vec{v}) I[f](t, \vec{v}) d\vec{v}.$$

$$(6)$$

Due to the fact that elements K_j are uniform, all basis functions $\phi_{i;j}(\vec{u})$ can be obtained from a single set $\phi_i(\vec{u})$ by a shift, $\phi_{i;j}(\vec{u}) = \phi_i(\vec{u} + \vec{w}_j)$. In [3], the bilinear convolution form of the Galerkin projection of the collision operator was introduced

$$I_i(\vec{w}) = \frac{8}{\omega \Delta \vec{v}} \int_{\mathbb{R}^3} \int_{\mathbb{R}^3} f(\vec{v} - \vec{w}) f(\vec{u} - \vec{w}) A(\vec{v}, \vec{u}, \phi_i), \tag{7}$$

where, in the case of inverse k-th power forces between particles,

$$A(\vec{v}, \vec{u}; \phi_i) = \frac{|g|^{\alpha}}{2} \int_{\mathbb{S}^2} (\phi_i(\vec{u}') + \phi_i(\vec{v}') - \phi_i(\vec{u}) - \phi_i(\vec{v})) b_{\alpha}(\theta) d\sigma.$$

Here $\alpha = (k-5)/(k-1)$ and all results obtained in the paper correspond to $\alpha = 1$ known as the hard sphere model. We note that $I_{\phi_{i;j}}$ is recovered from $I(\vec{w})$ by a substitution of the corresponding \vec{w}_j , namely $I_{\phi_{i;j}} = I_i(\vec{w}_j)$.

Integrals in (7) are discretized using Gauss quadratures native to the nodal-DG method yielding a discrete convolution form of the collision operator:

$$I_{i;j} := I_i(\vec{w}_j) = \sum_{i',i''=1}^{s^3} \sum_{j',j''=1}^{M^3} f_{i';j'-j} f_{i'';j''-j} A_{i,i',i'';j',j''}$$
(8)

where $f_{i';j'-j} = f(t, \vec{v}_{i';j'} - \vec{w}_j)$, $A_{i,i',i'';j',j''} = A(\vec{v}_{i';j'}, \vec{v}_{i'';j''}; \phi_i)(\omega_{i'}\Delta\vec{v}/8)(\omega_{i''}\Delta\vec{v}/8)$ and the three dimensional indices i' and i'' run over the velocity nodes within a single velocity cell and indices j' and j'' run over all elements K_j . We note that some shifted indices j' - j point outside of the velocity domain and the values of the solution outside of the domain are substituted with zeros. The discrete convolution form can be evaluated directly with $O(s^9M^8)$ operations as in [1, 2]. To derive a faster method [5], all discrete arrays are extended periodically and the discrete Fourier transform is applied resulting in a reduction of one sum:

$$\mathcal{F}[I_i]_p = M^3 \sum_{i',i''=0}^{s^3} \sum_{l=0}^{M^3-1} \mathcal{F}^{-1}[f_i']_{p-l} \mathcal{F}^{-1}[f_i'']_l \mathcal{F}[A_{i,i',i''}]_{p-l,l}$$
(9)

where $\mathcal{F}^{-1}[f_i]_p$ is the inverse discrete Fourier transform of discrete solution $f_{i;j}$ in index j and $\mathcal{F}[A_{i,i',i''}]_{p',p''}$ is the discrete Fourier transform of A(i,i',i'',j',j'') in indices j' and j''. Formula (9) leads to the development of $O(s^9M^6)$ method for evaluation of the collision operator. The method parallelizes effectively in indexes i,i',i'' providing scalability. The assumption of periodicity and the use of Fourier transform potentially introduces aliasing in solutions. To minimize aliasing while keeping accuracy, the domain should be selected sufficiently large so that the diameter of solution's support is approximately half of the linear domain size. This leads to a waste of degrees of freedom in the numerical scheme. Nevertheless, solutions can be computed at least two orders of magnitude faster than with the $O(s^9M^8)$ direct convolution approach for s=1,3, M>30. Additional comparison of the two methods can be found in [5]. In this paper, the Fourier convolution approach is used to compute the collection of training solutions described in the next section while the direct convolution is used for offline computations of the discrete kernels of the ROMs.

2.3. Class of solutions and solution collection. The class of solutions for which the ROM is constructed consists of solutions to the problem of spatially homogeneous relaxation with the initial data given by two homogeneous Gaussian densities. The initial data is normalized so that the velocity distribution function has unit density, zero bulk velocity and a set temperature. In the simulations presented in this paper, the value of dimensionless temperature .2 was used. The value of the temperature is selected so as to reduce aliasing in the scheme (9) above. The bulk velocities of the homogeneous Gaussian densities have zero v_2 and v_3 components, thus the solutions are radially symmetric in v_2v_3 -velocity plane.

A collection of solutions is computed by randomly generating macroscopic parameters of density, the v_1 components of the bulk velocity, and temperatures of two homogeneous Gaussian densities and solving (5) until a steady state is reached. The numerically computed velocity distribution functions are saved at multiple instances in time, each save becoming a data point in the collection.

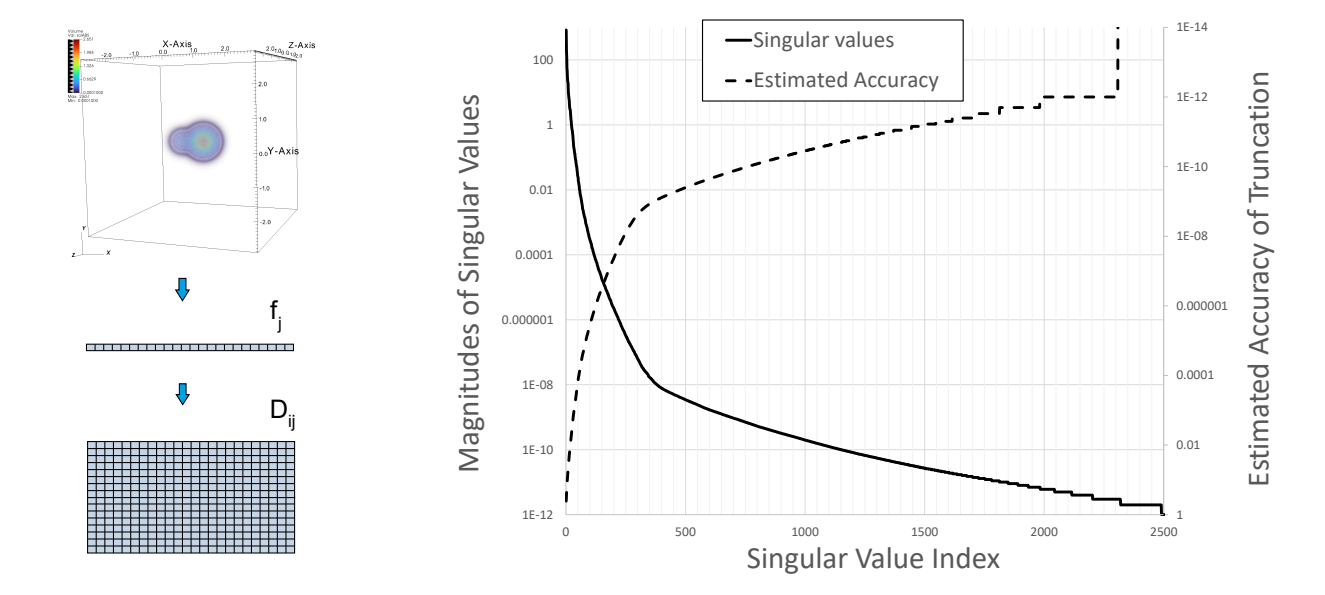


FIGURE 1. (left) Constructing the training solution data matrix: 3V solutions are reshaped into vectors f_j which are then stacked as rows of the solution data matrix D_{ij} . (right) Singular values of the solutions data matrix and estimated accuracy in Frobenius norm plotted on logarithmic scale.

We note that due to normalization of the initial data, the steady state is the same for all computed solutions.

The saved discrete solutions are re-arranged as one dimensional arrays f_j . Then f_j are added as rows to the matrix D_{ij} , where index i runs over all saved solutions and index j runs over all discretization points. This process is schematically depicted in Figure 1.

Singular values of matrix D_{ij} , i = 1, ..., P, $j = 1, ..., M^3$, M = 41, $P \approx 5000$, are shown in Figure 1. About 100 of cases of initial data are included in the results in Figure 1. It can be seen that the singular values decrease very fast allowing for low rank approximation \hat{D}_{ij} of the data matrix D_{ij} :

$$\hat{D}_{ij} = \sum_{l=1}^{K} \sigma_l \mu_i^l \xi_j^l \,. \tag{10}$$

Here σ_l is the l-th singular value, μ_i^l is the l-th left singular vector and ξ_j^l is the l-th right singular vector of D_{ij} . Vectors ξ_j^l represent orthogonal modes in solutions and σ_l represents the relative importance of these modes in the solution data. A SVD truncation theorem of numerical linear algebra states that the relative L^2 norm of error of approximating D_{ij} with a truncated sum (10) is 3.68E-3 for K=16, 1.63E-4 for K=35, and 1.74E-5 for K=53. The relative Frobenius norm of the SVD truncation is given by the quantity $e_K = (\sum_{i=K+1}^P \sigma_i^2)^{1/2}/(\sum_{i=1}^P \sigma_i^2)^{1/2}$. Values of e_K for K=16, 27, 35, 42, and 53 are 6.71E-3, 1.14E-3, 3.51E-4, 1.53E-4, and 4.27E-5, respectively. This suggests that training solutions can be approximated accurately with first 35 singular vectors ξ_j^l and these vectors provide a very efficient basis for representing this class of solutions (but not other classes of solutions).

2.4. Reduced Order Model for the Boltzmann equation. Assuming that an unknown solution is represented by the training collection, a ROM can be readily obtained from lower rank approximation (10). We define matrix $H_{lj} = \xi_j^l$ that provides a linear projection mapping from the space \mathbb{R}^{M^3} where discrete solutions reside to the lower dimensional space \mathbb{R}^K , $K \ll M^3$ of coefficients y_l of linear combinations of first K singular vectors ξ_j^l . In particular, $y_l = \sum_{j=1}^{M^3} H_{lj} f_j$ and $\hat{f}_j = \sum_{l=1}^K H_{lj} y_l$. Substituting the approximation \hat{f}_j in (8) and applying projection H_{lj} we obtain our first ROM (here we assume s = 1 for simplicity, although a generalization is straightforward):

$$\partial_t y_k = \partial_t \left(\sum_{j=1}^{M^3} H_{kj} f_j \right) = \sum_{j=1}^{M^3} H_{kj} \sum_{j'=1}^{M^3} \sum_{j''=1}^{M^3} \left(\sum_{k'=1}^K H_{k',j'-j} y_{k'} \right) \left(\sum_{k''=1}^K H_{k'',j''-j} y_{k''} \right) A_{j',j''}$$

$$= \sum_{k'=1}^K \sum_{k''=1}^K y_{k'} y_{k''} \hat{A}_{k',k'',k}$$
(11)

where

$$\hat{A}_{k',k'',k} = \sum_{j=1}^{M^3} H_{kj} \sum_{j'=1}^{M^3} \sum_{j''=1}^{M^3} H_{k',j'-j} H_{k'',j''-j} A_{j',j''}$$
(12)

We note that for fixed values of k, k', k'', the two internal sums are identical to (8). As a result, the three index array $\hat{A}_{k',k'',k}$ is pre-computed using either direct convolution or the Fourier convolution approaches. Modifications of the existing nodal-DG solver [5] to compute $\hat{A}_{k',k'',k}$ are minimal.

There are two alternative formulations of ROM (11) that are of interest. First, we can use the fact that the exact collision operator vanishes on homogeneous Gaussians and replace (11) with

$$\partial_t y_k = \sum_{k',k''=1}^K (y_{k'} + w_{k'})(y_{k''} - w_{k''})\hat{A}_{k',k'',k}$$
(13)

where w_k is the ROM projection of the steady state solution. The difference between (11) and (13) is the term

$$\sum_{k'=1}^{K} \sum_{k''=1}^{K} w_{k'} w_{k''} \hat{A}_{k',k'',k}$$

that is theoretically expected to converge to 0 as $K \to \infty$ and as we increase the number of points in the underlying nodal-DG discretization. In practice, however, the term is not expected to converge due to accumulation of roundoff errors. In fact, this term is not small for the ROM approximations of the steady state solution and subtraction of this term has been known to improve approximations for solutions that are near the steady state. As a result, in simulations presented in the next section, this form of ROM is used.

The second modification is due to the fact that w_k is time independent and thus $\partial_t w_k = 0$. Introducing $e_k = y_k - w_k$, we rewrite (13) as

$$\partial_t e_k = \sum_{k'=1}^K B_{k',k} e_{k'} + \sum_{k',k''=1}^K e_{k'} e_{k''} \hat{A}_{k',k'',k} , \qquad (14)$$

where $B_{k',k} = 2\sum_{k''=1}^K \hat{A}_{k',k'',k} w_{k''}$. One can see that $e_k = 0$ is a solution of this system.

One option is to implement the entire solver in the ROM basis using either (11), (13), or (14). However, in this paper, ROMs (11), (13), and (14) are used inside the fully discretized nodal-DG solver as subroutines for fast evaluation the collision operator. Specifically, in each call of the subroutine, projection of the solution $y_k = \sum_{j=1}^{M^3} H_{kj} f_j$ is computed. Then, either (11), (13), or (14) is used to evaluate $\partial_t y_k$. Finally, the recovery $\hat{I}_j = \sum_{l=i}^K \partial_t y_l H_{lj}$ is used to approximate the value of the collision operator. The resulting method has complexity $O(K^3) + O(KM^3)$, which is intractable for $K > 10^4$, but yields significant acceleration when $K^3 \ll M^6$.

Evaluation of arrays $\hat{A}_{k',k'',k}$ and $B_{k',k}$ represents the offline stage of the ROMs. Computational costs for $\hat{A}_{k',k'',k}$ and $B_{k',k}$ are equivalent to costs of evaluating K^2 and K collision operators, respectively. In practice, computations of these arrays for M=41 grid resolution and K=65 takes about 10 hours on an XSEDE's Bridges HPC compute node using the Fourier convolution approach. Direct convolution approach does not introduce aliasing errors, and was used for basis functions with large supports, resulting in about 100 times slower computations. However, the implemented scalable MPI parallelization of the code allows to achieve comparable wall times. Updating the ROM basis, e.g., when an outlier is encountered, requires re-evaluation of components of $\hat{A}_{k',k'',k}$ and $B_{k',k}$. It is expected to be more time consuming than computing solutions using the full discretization of the collision operator and is not practical in the online stage. As a result, the approach is most useful for cases when many similar flows need to be computed cheaply, e.g., in grid parameter searches or parameter optimization.

3. Numerical Results

In this section we discuss results of applying ROM (13), (12) to the solution of the problem of spatially homogeneous relaxation. Our first numerical experiment is concerned with estimating errors caused by projecting the solutions and the collision operator to the ROM basis formed by singular vectors of the data matrix D_{ij} . Benchmark solutions for this experiment are computed using a nodal-DG formulation [5] on 41³ grid points. In the following, solutions are identified by their deviation from continuum at the initial time using the quantity $\varepsilon = ||f(0, \vec{v}) - f^M(\vec{v})||_{L^1}$, where $f^{M}(\vec{v})$ is the homogeneous Gaussian density with the same macroscopic density, bulk velocity, and temperature as $f(t, \vec{v})$. In Table 1, relative L^1 errors in approximate solutions and collision operators are computed for different sizes of ROM bases for four randomly selected cases of initial data identified by $\varepsilon = .1, .24, .29,$ and 1.1. Values $\varepsilon = .1, .24,$ and .29 represent medium deviations from continuum, and value $\varepsilon = 1.1$ represents strong deviation from continuum. The first two solutions presented in Table 1 ($\varepsilon = .29$ and $\varepsilon = 1.1$) are part of the dataset used to develop the ROM model. The last two solutions ($\varepsilon = .24$ and $\varepsilon = .1$) were generated after the ROM was trained. Thus, while they belong to the same class of solutions, these solutions were not used to build the ROM. In total, ten randomly picked training solutions and ten randomly generated new solutions were reviewed for accuracy and the results were consistent with those included in Table 1.

It can be observed in Table 1 that, for the first two solutions, errors of the ROM approximations decrease consistently with the SVD truncation estimates. In particular, as the size of the truncated SVD basis is increased from 16 to 53, the errors decrease by two orders of magnitude. Errors of approximating the collision operators are one order larger than for the corresponding solutions. Nevertheless, the errors decrease with same rate. In contrast, the errors for the last two solutions decrease only by one order of magnitude. It is not surprising: since the latter solutions are not

included in the ROM training data, it is likely that these solutions are on the margins of the cases that are familiar to the ROM and that the SVD basis may not be rich enough to approximate it asymptotically. That is, we expect that non-negligible components are present in these solutions that are orthogonal to the space spanned by the training data. One can see that errors are larger for the $\varepsilon = .24$ solution than for the $\varepsilon = .1$ solution. This suggests that the $\varepsilon = .1$ solution fell withing the cases that are familiar to the ROM while the $\varepsilon = .24$ solution is an outlier. We note that larger values of ε do not, in general, result in larger approximation errors. Instead, large approximation errors happen when ROM encounters a case that is not covered by its basis. Only about 100 cases of randomly initialized solutions were used to train the ROM. This, evidently, is not sufficient to achieve good coverage of the solution manifold. It is expected that one could improve the approximating properties of the ROM by increasing the size of the training data set. However, it not clear how many random samples are needed to guarantee asymptotic convergence with high probability for a randomly generated set of initial data. In all cases, convergence of approximations of the collision operators follows the convergence of solutions, which suggests that slow convergence of approximations of solutions could be used as a predictor of poor approximation of the collision operator by the ROM.

	$\varepsilon = .29$		$\varepsilon = 1.1$		$\varepsilon = .24$		$\varepsilon = .1$	
_ k	sol.	coll. op.	sol.	coll. op.	sol.	coll. op.	sol.	coll. op.
		1.82E-1						
27	1.66E-2	7.58E-2	1.35E-2	3.37E-2	4.34E-2	2.24E-1	1.71E-3	2.41E-2
		2.05E-2						
42	1.13E-3	1.13E-2	1.42E-3	6.98E-3	1.69E-2	9.39E-2	4.07E-4	9.41E-3
53	3.69E-4	3.97E-3	5.15E-4	2.34E-3	1.31E-2	4.68E-2	1.32E-4	3.22E-3

Table 1. Relative L^1 errors in approximating solutions and the corresponding collision operators in truncated singular value bases.

In Figures 2 and 3 results are plotted for solving the problem of spatially homogeneous relaxation using ROM. In Figure 2 relaxations of directional temperatures and third moments are compared to those of solutions computed using fully discretized Boltzmann equation [5]. The moments are defined as $f_{v_i,p} = \int_{\mathbb{R}^3} (v_i - \bar{v}_i)^p f(t, \vec{v}) dv$, $i = 1, 2, p = 2, 3, \vec{v} = (v_1, v_2, v_3)$. Initial data for solutions in these plots was generated after the ROM was constructed. That is, the ROM does not include data from these solutions. The last two solutions from Table 1 are included in the plots. It can be seen that approximations obtained by ROM model are very accurate. Not shown here, differences could be observed in sixth moments, however, overall, the solutions achieve very good accuracy. The computational speedup achieved by the ROM is summarized in Table 2. The time is measured for a single threaded evaluation on Bridges HPC regular compute nodes (2 Intel Haswell E5-2695 v3 CPUs with 14 cores per CPU, 2.3-3.3 GHz). Overall, at least two orders of magnitude of speedup were observed. These CPU times also show significant improvement compared to times reported in [26] for a fast spectral method. However, for a fair comparison, we also need to consider costs of building the ROM, which in our case include several thousands of evaluations of collision operator using full discretizations and are significant. As a result, the approach is only suited for problems in which many like simulations need to be performed, for

example, during a parameter grid search. For such problems, costs of training the ROM can be offset by the savings of computing the collision operator.

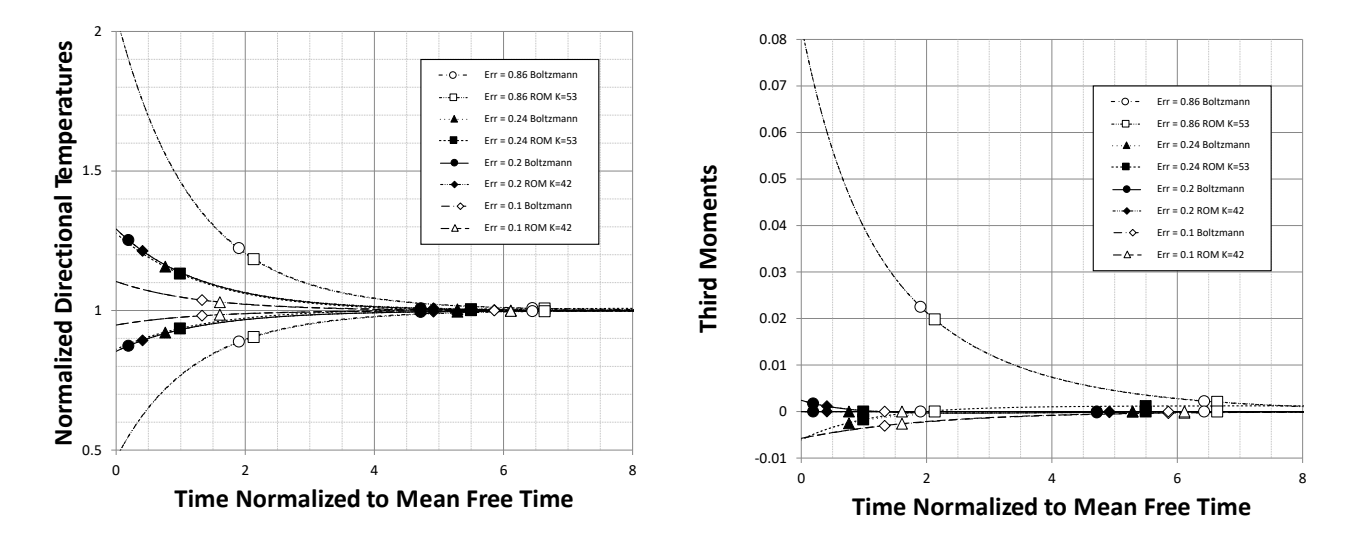


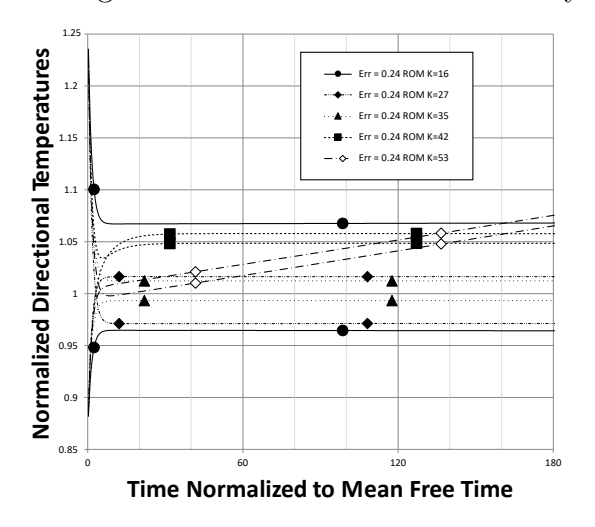
FIGURE 2. Relaxation of moments $f_{v_i,p} = \int_{\mathbb{R}^3} (v_i - \bar{v}_i)^p f(t, \vec{v}) dv$, $i = 1, 2, p = 2, 3, \vec{v} = (v_1, v_2, v_3)$.

k	CPU time, s	Speedup vs. $O(M^6)$, 151 sec	Speedup vs. $O(M^8)$, 31116 sec
16	.11	1.37E+3	2.82E+4
27	.19	7.75E+2	1.60E+4
35	.21	7.31E+2	1.51E+4
42	.27	5.42E+2	1.12E+4
53	.35	4.31E+2	8.89E + 3

TABLE 2. Speedup in evaluating one instance of collision operator using ROM. Comparisons are made to the CPU times for evaluating the collision operator on the mesh with 41^3 grid points using the nodal-DG Fourier transform based approach with $O(M^6)$ complexity (151 seconds average) and the direct convolution nodal-DG approach with $O(M^8)$ complexity (31116 seconds estimated). Here M is the number of velocity points in one velocity dimension.

In Figure 3, the long term behavior of directional temperatures in ROM solutions is considered. The presented solutions correspond to the last two cases of initial data included in Table 1: solutions corresponding to the initial data with $\varepsilon = .24$ are presented in the left plot, and solutions with $\varepsilon = .1$ in the right plot. All solutions are computed using ROM (13), (12) with different sizes of the ROM basis. According to Table 1, approximation errors in the case of $\varepsilon = .24$ are larger. As a result, the solutions are expected to be less accurate than the solutions for $\varepsilon = .10$ data. This indeed is the case, as the left plot shows a considerably larger errors in the steady state solutions. It can be seen, however, that in both cases, solutions with K = 16, 27, 35, and 42 reach steady states away from the theoretically predicted states. In the case of K = 53, a linear

instability is present in both plots, but is more prominent in the case of $\varepsilon = .24$. Noticeably, in this case, linear growth of energy and nonlinear growth of density are observed. We will attempt to investigate causes of this linear instability next.



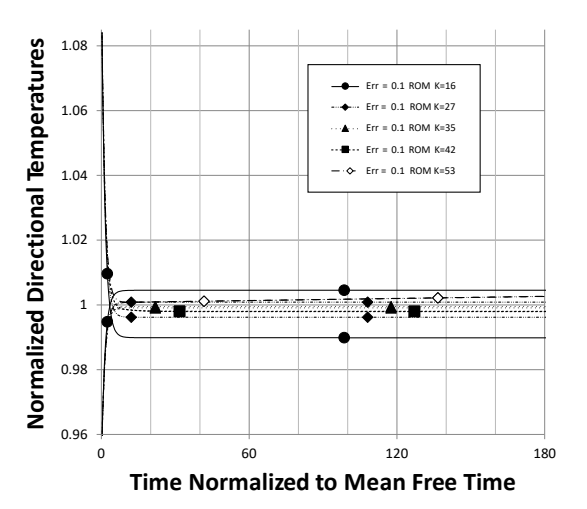


FIGURE 3. Long term behavior of directional temperatures in ROM solutions. Two cases of initial data: (left) $\varepsilon = .24$; (right) $\varepsilon = .1$.

To understand the source of instability in ROM solutions, we take a closer look at formula (14), which is equivalent to (13). In Figure 4, largest real parts of eigenvalues of matrix $B_{k',k}$ are plotted as functions of the ROM size (triangles). One can see that for K < 47, all eigenvalues have strictly negative real parts and at least one eigenvalue has real part that is close to zero. For $K \geq 48$, eigenvalues with positive real parts are present making the $e_k = 0$ solution unstable. The presence of these eigenvalues explains the unstable mode in Figure 3 for K = 53.

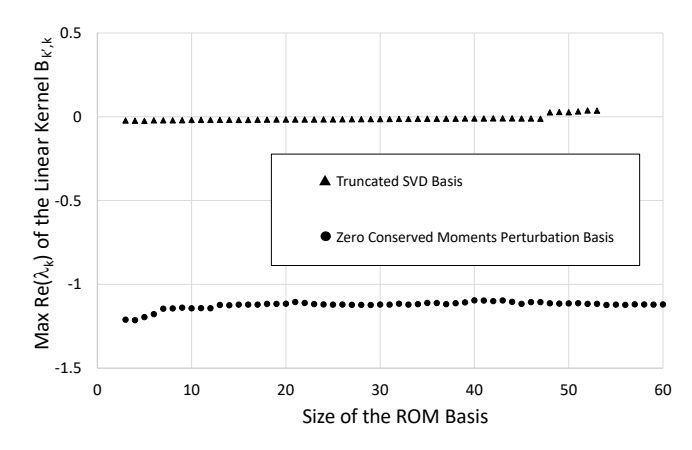


FIGURE 4. Largest real parts of eigenvalues of the matrices $B_{k',k}$ for the ROM basis of truncated singular vectors (triangles) and the zero conserved moments perturbation basis (circles).

To understand the non-physical long term steady state values in Figure 3, it is informative to consider the portion of the solution that is not captured by the ROM basis. In Figure 5, the

difference between the steady state ROM solution and the exact solution is compared to the error in approximating the initial data in the ROM basis for the case of K=35. One can see that the two errors are very similar, with the differences explainable by truncation errors in the model including small errors in conservation that accumulated over 2.0E+5 time steps of the simulation.

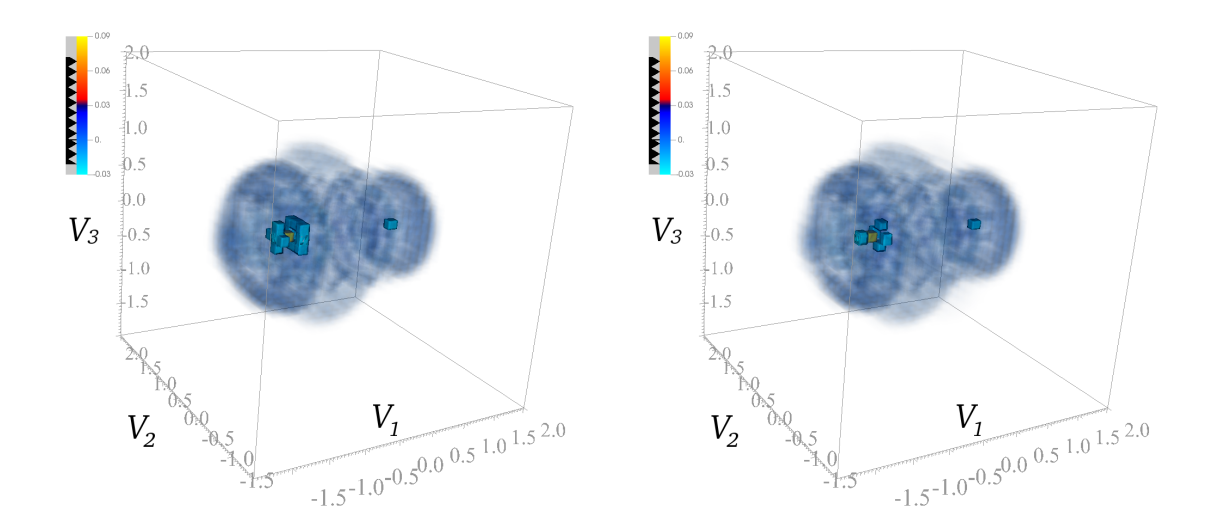


FIGURE 5. Failure of the ROM basis to capture the $\varepsilon = .24$ solution in the case of K = 35: (left) difference between the long term steady state ROM solution and the exact solution; (right) ROM residual in the initial data.

In Table 3, moments of the errors in the ROM projections of the initial data are shown for $\varepsilon=.24$ solution for different sizes of the ROM basis, including the case presented in Figure 5. While the density, n, of the projection error is less than a percent of the total solution density, other moments have large values. When combined with the ROM solution using known formulas, these moments cause the non-physical values seen in Figure 3. Another important observation is that the non-vanishing ROM projection errors affect the conserved moments. In particular, the density, bulk velocity, and temperature of the ROM projection are not equal to those of the full solution. To circumvent the non-physical steady state values, long term instability for large ROM sizes, and loss of conservation, a modified ROM model can be proposed based on formulation (14) as is discussed next.

\underline{k}	n	\bar{v}_1	T	$\int f_{v_1,2}$	$f_{v_2,2}$	$f_{v_1,3}$
16	-4.34E-3	04	.24	89	.56	1.13
27	2.87E-3	35	.21	61	.41	.69
35	1.29E-3	-1.32	91	-1.65	.37	-9.33
42	5.47E-3	-1.87E-2	.94	.33	.30	22

TABLE 3. Moments of the ROM residuals in the initial data of $\varepsilon = .24$ solution. Here n is the formal density, \bar{v}_1 is the v_1 component of the formal bulk velocity, T is the formal temperature, and $f_{v_i,p} = \int_{\mathbb{R}^3} (v_i - \bar{v}_i)^p f(t, \vec{v}) dv$.

3.1. Zero Conserved Moments Perturbation Basis. Consider a version of the ROM that is based on formulation (14), but introduces modifications to both the truncated SVD basis and the evolution equations. Specifically, we will add the discrete representation f_j^M of the exact steady state $f^M(\vec{v})$ as the first basis vector of the new ROM basis. Clearly, singular vectors ξ_j^i are not orthogonal to f_j^M . Starting with the f_j^M , the Gram-Schmidt orthogonalization is performed to obtain a new set of orthogonal vectors. It was observed that the new vectors have non-zero conserved moments. Beginning from the second vector, corrections are introduced to each vector to nullify their conservative moments while keeping it orthogonal to the first vector, that is, to the steady state solution. To minimize the effect of the conservative correction on the support of the basis vectors, corrections are only introduced in the components that are larger than .01 in magnitude. After the correction is introduced, the system is orthogonalized one last time and the first vector is removed producing the final zero conserved moments perturbation (ZCMP) ROM basis.

In ZCMP ROM, the problem of spatially homogeneous relaxation is solved by evolving the deviation of the solution from the steady state, $g(t, \vec{v}) := f(t, \vec{v}) - f^M(\vec{v})$. The steady state solution is a Maxwellian distribution $f^M(\vec{v})$ with mass, momentum, and temperature being the same as of the initial data. By construction, the first basis function represents the steady state; as a result, the coefficient of the first basis function is simply kept constant during simulation. Values of $g(t, \vec{v})$ are decreasing with time eventually leaving the Maxwellian as the steady state solution.

Furthermore, the deviation $g(t, \vec{v})$ is split into two parts, $g(t, \vec{v}) = g_{\text{ROM}}(t, \vec{v}) + g_{\perp}(t, \vec{v})$, where $g_{\text{ROM}}(t, \vec{v})$ is the projection of $g(t, \vec{v})$ onto the ZCMP basis and $g_{\perp}(t, \vec{v})$ is its orthogonal complement. Evolution for $g_{\text{ROM}}(t, \vec{v})$ is given by (14), with the projection matrix H_{kj} and arrays $\hat{A}_{k',k'',k}$ and $B_{k',k}$ corresponding to the ZCMP basis. Following the ideas of [17, 56, 18], evolution of $g_{\perp}(t, \vec{v})$ is simply an exponential decay

$$\partial_t g_{\perp}(t, \vec{v}) = -\nu g_{\perp}(t, \vec{v}),$$

where ν is the dimensionless collision frequency $\nu(t, \vec{x})$ of the ES-BGK model [33],

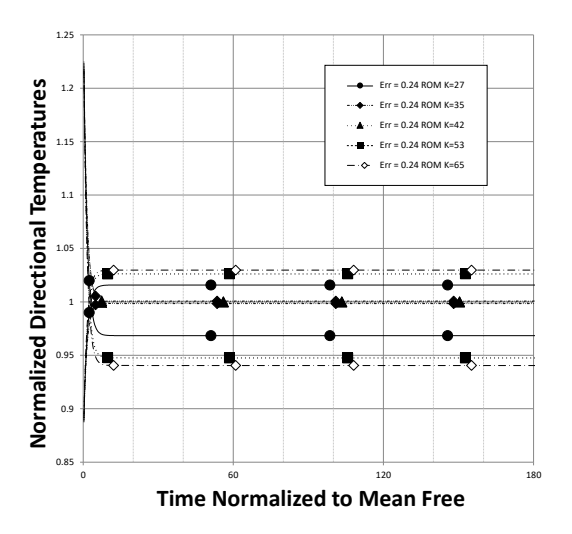
$$\nu = \frac{N_{\infty}\kappa\sqrt{T_{\infty}}}{L_{\infty}^2\sqrt{2R}} \frac{nT}{(1-\alpha)\mu}$$
 (15)

Here μ is the gas viscosity, α is the parameter that controls the Prandtl number of the ES-BGK model; constants T_{∞} , N_{∞} , and L_{∞} are related to the dimensionless reduction and represent reference dimensional temperature, number density, and characteristic length, respectively; κ is the Boltzmann constant; and R is the normal gas constant.

We note that the ZCMP ROM is conservative by construction. We recall that $g(t, \vec{v})$ has zero mass, momentum, and energy. By forcing basis functions of the ZCMP ROM to also have zero mass, momentum, and energy, one guarantees that both the ZCMP ROM portion of the solution $g_{\text{ROM}}(t, \vec{v})$ and the projection residual $g_{\perp}(t, \vec{v})$ are free from violations of constraints up to round-off errors. Additional ideas to enforce conservation laws in Galerkin methods with globally supported bases can be found in [28, 61, 34, 51].

The first benefit of removing the steady state solution from the ROM (14) is that the solutions become stable for large sizes of the ROM. In Figure 4, largest real parts of the eigenvalues of the matrix $B_{k',k}$ are presented for the ZCMP basis (circles). The real parts remain below -1 for K > 48. In Figure 6, long term behavior of the ZCMP ROM solutions is considered. The

left figure corresponds to keeping the orthogonal complement $g_{\perp}(t, \vec{v})$ constant, while the right figure corresponds to damping $g_{\perp}(t, \vec{v})$ exponentially in time using (15). In both cases, no growing instabilities are observed in the solutions even when sizes K = 53 and K = 65 were used for the ZCMP ROM. We can still observe the non-physical steady-state values in the plots on the left. However, it is clear that these values are caused by the non-vanishing component g_{\perp} . In the simulations presented in the right plot, the component g_{\perp} decays exponentially and the non-physical values are not present.



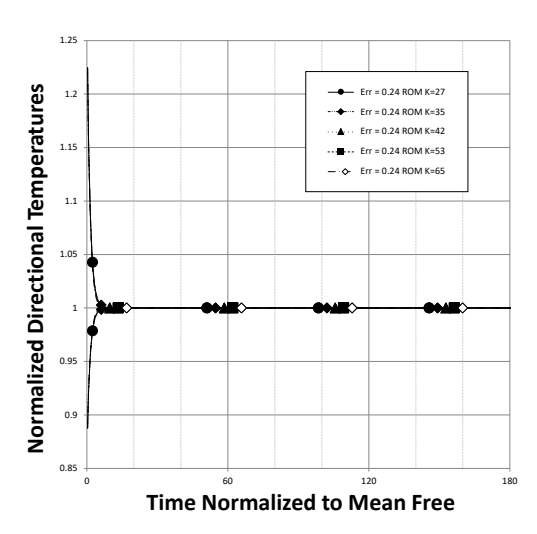
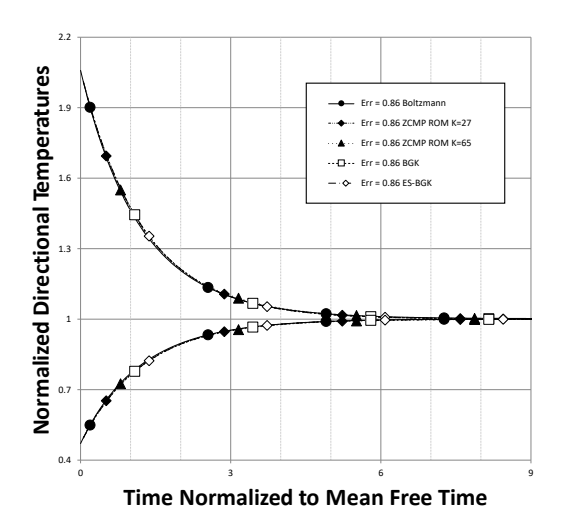


FIGURE 6. Long term behavior of directional temperatures in ZCMP ROM solutions for $\varepsilon = .24$ initial data. (left) Component g_{\perp} is kept constant. (right) Component g_{\perp} is damped exponentially in time.

In conclusion, we compare solutions obtained by the ZCMP ROM with damping to those obtained by the classical Bhatnagar-Gross-Krook (BGK) [12] and the ellipsoidal-statistical BGK (ES-BGK) [33] models. In Figure 7 relaxation of the second and third moments are presented for the case of initial data with $\varepsilon = .86$. It can be observed that the relaxation of the second moments is very accurately captured in all simulations. For the third moments, the ZCMP ROM solutions are superior to the BGK and ES-BGK models. Not shown here, the results for fourth and higher models are mixed with the BGK model sometimes being more accurate then the ZCMP ROM.

The computational costs for the ZCMP ROM K=27 solution is about two times faster than the BGK and ES-BGK models, while for K=65 is about four times slower. It should be noted, however, that both BGK and the ES-BGK models, while capturing the second moments accurately, do not produce correct distributions $f(t, \vec{v})$. This fact is illustrated in Figure 8 where $v_3=0$ cross sections of solutions are presented at about two mean free times mark. Plot (a) shows the cross section of the solution to the Boltzmann equation, while plots (b), (c) and (d) show the differences between the solution to the Boltzmann equation and the BGK, ZCMP ROM for K=27 and K=65 solutions, respectively. It it observed that the BGK solution has areas with 3.7% error, while ZCMP ROM solutions have maximum error at about .55%. As a result, ZCMP ROM solutions reproduce the velocity distribution function more accurately.

Another observation about the ROM solutions is that solutions with larger size of the basis, say K = 65, produce less accurate values of moments then solutions for moderate size of the basis,



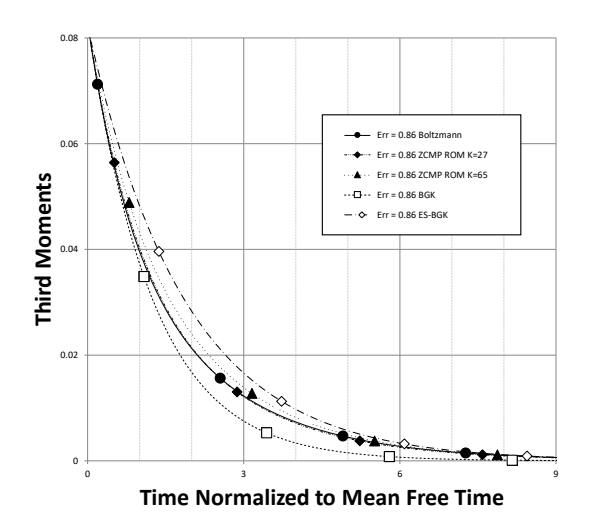


FIGURE 7. Relaxation of second and third moments in solutions obtained by the BGK model, the ES-BGK model, and the ZCMP model for sizes of the bases K=27 and K=65. A solution to the Boltzmann equation is included for comparison. All solutions correspond to the case of initial data $\varepsilon=.86$.

K=27. An example of accuracy loss can be seen in Figure 7 for the third moments computation. The reason for such loss of accuracy could be elucidated from Figure 8(c) and (d) where the errors of approximating the Boltzmann solutions by the ZCMP ROM are presented for two different sizes of the basis, K=27 and K=65. It was observed, that as the order number of the ROM basis vector increases, its support expands and the basis vector becomes more oscillatory. It can be seen in Figure 8(c) and (d), that K=65 solution has a region of small errors, less than .05% that stretch further out than that of the K=27 solution. This problem seems to affect more the solutions that are outliers with respect to the ROM training data. It appears that third moments in Figure 7 are sensitive to these small perturbations.

The observed perturbations of solutions for large sizes of the ROM bases are likely caused by oscillatory nature of the high order basis functions and the way the ROM residual g_{\perp} is treated. Initially, oscillations in the high order basis functions are "canceled out" by matching oscillations in the residual resulting in a smooth solution. Once the residual starts to decay exponentially with frequency given by (15), the residual and the solution are no longer "in sync". In particular, it appears that the residual is driven to zero at a rate faster than its counterpart in the ZCMP ROM model. As a result, oscillations in the high order basis functions no longer cancel, producing the observed perturbations in high order moments. A possible workaround to this problem could be a more sophisticated procedure to treat the residual g_{\perp} . In particular, one could try to deduce a "correct" relaxation rate by averaging eigenvalues of the matrix $B_{k',k}$. Alternatively, a smoother basis functions or a filtering technique could be proposed to reduce pollution by these small oscillations. Addressing the nonphysical oscillations would be even more important in spatially dependent simulations and will be the authors' future work.

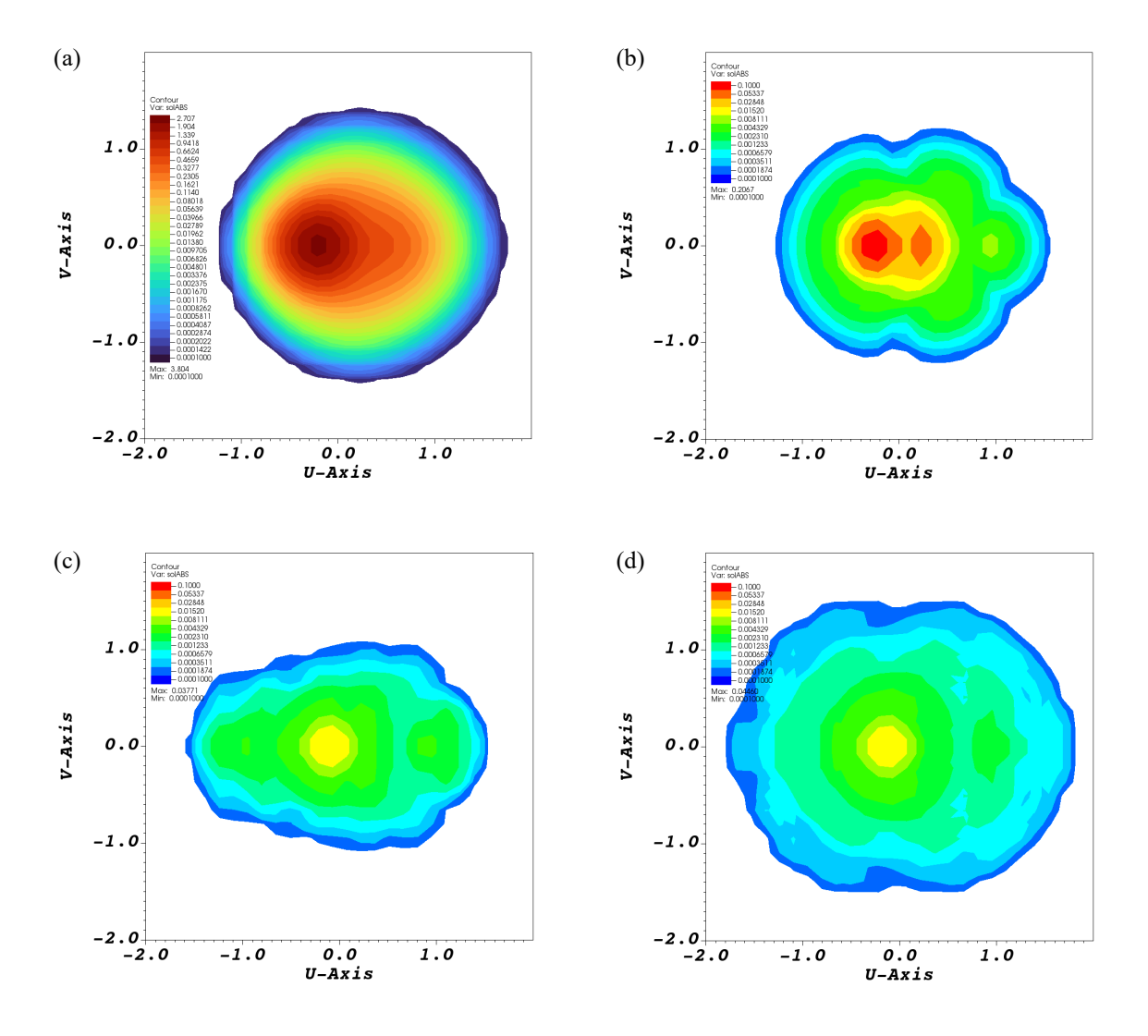


FIGURE 8. Spatially homogeneous relaxation of initial data with $\varepsilon = .86$ captured at about two mean free times mark. (a) The $v_3 = 0$ cross section of the solution to the Boltzmann equation. (b), (c), and (d) The $v_3 = 0$ cross sections of absolute values of the differences between the Boltzmann and the BGK solutions, (b); the ZCMP ROM K = 27 solutions, (c); and the ZCMP ROM K = 65 solutions, (d).

4. Conclusions

We had developed, implemented, and tested reduced order models (ROMs) for the spatially homogeneous Boltzmann equation for a class of solutions corresponding to relaxation of a mixture of two homogeneous Gaussian streams. The first ROM is constructed by performing a SVD decomposition and SVD truncation of the solution data matrix. The second ROM is constructed by augmenting the truncated SVD basis by adding the steady state solution and enforcing conservation. The measured speedup of the ROM as compared to the underlying full discrete formulation

is at least two and as high as three orders of magnitude. The ROM provides accurate representation of solutions although some perturbations in high order moments could be traced to the way the approach handles ROM residuals. The future authors work will include improving residual damping procedures and design of smoother basis functions. The presented approach is best suited for problems where many like simulations need to be performed, e.g., during a grid search optimization. The reason for that are the considerable costs of off-line training of the ROM, the process that requires many evaluations of the collision operator done beforehand. This, in particular means that the method can only be applied to problems for which solutions could be obtained by other means. However, the approach will significantly accelerate the solutions once sufficient data about the problem is gathered. The approach could be potentially used for simulations of complex flows if local features of the flows could be reproduced on a smaller scale in order to train the ROM. Another possible solution is to attempt model training online by studying solution dynamics. Development of these approaches will be the authors' future work.

5. Acknowledgment

The first and third authors were supported by AFIT and Air Force Office of Scientific Research grant F4FGA08305J005. The first author was also supported by NSF DMS-1620497 and DMS-2111612 grants. The second author was supported by Air Force Office of Scientific Research under Award Number FA9550-20QCOR100 (PO: Fahroo). The research was supported in part by the Air Force Research Laboratory Propulsion Directorate, through the Air Force Office of Scientific Research Summer Faculty Fellowship Program, Contract Numbers FA8750-15-3-6003, FA9550-15-0001 and FA9550-20-F-0005. Computational resources were provided by the Extreme Science and Engineering Discovery Environment (XSEDE) [54], which is supported by National Science Foundation grant number ACI-1548562.

REFERENCES

- 1. A. Alekseenko and E. Josyula, *Deterministic solution of the Boltzmann equation using a discontinuous Galerkin velocity discretization*, 28th International Symposium on Rarefied Gas Dynamics, 9-13 July 2012, Zaragoza, Spain, AIP Conference Proceedings, American Institute of Physics, 2012, p. 8.
- 2. _____, Deterministic solution of the spatially homogeneous Boltzmann equation using discontinuous Galerkin discretizations in the velocity space, Journal of Computational Physics 272 (2014), no. 0, 170 188.
- 3. A. Alekseenko, T. Nguyen, and A. Wood, A deterministic-stochastic method for computing the Boltzmann collision integral in $\mathcal{O}(mn)$ operations, Kinetic & Related Models 11 (2018), no. 1937-5093_2018_5_1211, 1211.
- 4. Alexander Alekseenko, Amy Grandilli, and Aihua Wood, An ultra-sparse approximation of kinetic solutions to spatially homogeneous flows of non-continuum gas, Results in Applied Mathematics 5 (2020), 100085.
- 5. Alexander Alekseenko and Jeffrey Limbacher, Evaluating high order discontinuous Galerkin discretization of the Boltzmann collision integral in $\mathcal{O}(n^2)$ operations using the discrete Fourier transform, Kinetic & Related Models 12 (2019), no. 1937-5093_2019_4_703, 703.
- David Amsallem, Matthew J. Zahr, and Charbel Farhat, Nonlinear model order reduction based on local reducedorder bases, International Journal for Numerical Methods in Engineering 92 (2012), no. 10, 891–916.
- David Amsallem, Matthew J. Zahr, and Kyle Washabaugh, Fast local reduced basis updates for the efficient reduction of nonlinear systems with hyper-reduction, Advances in Computational Mathematics 41 (2015), no. 5, 1187–1230.
- 8. V. V. Aristov and S. A. Zabelok, A deterministic method for the solution of the Boltzmann equation with parallel computations, Zhurnal Vychislitel'noi Tekhniki i Matematicheskoi Physiki 42 (2002), no. 3, 425–437.
- 9. V.V. Aristov, Direct methods for solving the boltzmann equation and study of nonequilibrium flows, Fluid Mechanics and Its Applications, Kluwer Academic Publishers, 2001.

- 10. Hans Babovsky, Discrete kinetic models in the fluid dynamic limit, Computers & Mathematics with Applications 67 (2014), no. 2, 256 271, Mesoscopic Methods for Engineering and Science (Proceedings of ICMMES-2012, Taipei, Taiwan, 23–27 July 2012).
- 11. Hans Babovsky, *Translation invariant kinetic models on integer lattices*, AIP Conference Proceedings **1628** (2014), no. 1, 640–647.
- 12. P. L. Bhatnagar, E. P. Gross, and M. Krook, A model for collision processes in gases. i. small amplitude processes in charged and neutral one-component systems, Phys. Rev. 94 (1954), no. 3, 511–525.
- 13. A. V. Bobylev and S. Rjasanow, Numerical solution of the boltzmann equation using a fully conservative difference scheme based on the fast fourier transform, Transport Theory and Statistical Physics 29 (2000), no. 3-5, 289–310.
- 14. A.V. Bobylev and S. Rjasanow, Difference scheme for the boltzmann equation based on fast fourier transfrom, European Journal of Mechanics B/Fluids 16 (1997), no. 2, 293 306.
- 15. _____, Fast deterministic method of solving the boltzmann equation for hard spheres, European Journal of Mechanics B/Fluids 18 (1999), no. 5, 869 887.
- 16. Arnout M.P. Boelens, Daniele Venturi, and Daniel M. Tartakovsky, *Tensor methods for the boltzmann-bgk equation*, Journal of Computational Physics **421** (2020), 109744.
- 17. Zhenning Cai, Yuwei Fan, and Yanli Wang, Burnett spectral method for the spatially homogeneous boltzmann equation, Computers & Fluids **200** (2020), 104456.
- 18. Zhenning Cai and Manuel Torrilhon, Approximation of the linearized boltzmann collision operator for hard-sphere and inverse-power-law models, Journal of Computational Physics 295 (2015), 617–643.
- C. Cercignani, Rarefied gas dynamics: From basic concepts to actual caclulations, Cambridge University Press, Cambridge, UK, 2000.
- 20. G. Dimarco and L. Pareschi, Numerical methods for kinetic equations, Acta Numerica 23 (2014), 369-520.
- 21. Giacomo Dimarco, Rapha el Loubère, Jacek Narski, and Thomas Rey, An efficient numerical method for solving the boltzmann equation in multidimensions, Journal of Computational Physics **353** (2018), 46 81.
- 22. F. Filbet, C. Mouhot, and L. Pareschi, *Solving the Boltzmann equation in N* log₂ N, SIAM Journal on Scientific Computing **28** (2006), no. 3, 1029–1053.
- 23. E. Fonn, P. Grohs, and R. Hiptmair, *Hyperbolic cross approximation for the spatially homogeneous Boltzmann equation*, IMA Journal of Numerical Analysis **35** (2015), 1533–1567.
- 24. I. M. Gamba and S. H. Tharkabhushanam, Shock and boundary structure formation by spectral-Lagrangian methods for the inhomogeneous Boltzmann transport equation, Journal of Computational Mathematics (2010).
- 25. I.M. Gamba and C. Zhang, A conservative discontinuous Galerkin scheme with $O(N^2)$ operations in computing Boltzmann collision weight matrix, 29th International Symposium on Rarefied Gas Dynamics, July 2014, China, AIP Conference Proceedings, American Institute of Physics, 2014, p. 8.
- Irene M. Gamba, Jeffrey R. Haack, Cory D. Hauck, and Jingwei Hu, A fast spectral method for the Boltzmann collision operator with general collision kernels, SIAM Journal on Scientific Computing 39 (2017), no. 4, B658– B674.
- 27. Irene M. Gamba and Sergej Rjasanow, *Galerkin-petrov approach for the boltzmann equation*, Journal of Computational Physics **366** (2018), 341 365.
- 28. Irene M. Gamba and Sri Harsha Tharkabhushanam, Spectral-Lagrangian methods for collisional models of non-equilibrium statistical states, Journal of Computational Physics 228 (2009), no. 6, 2012–2036.
- 29. Philipp Grohs, Ralf Hiptmair, and Simon Pintarelli, Tensor-product discretization for the spatially inhomogeneous and transient Boltzmann equation in 2D, SMAI Journal of Computational Mathematics 3 (2017), 219–248.
- 30. Alexei Heintz, Piotr Kowalczyk, and Richards Grzhibovskis, Fast numerical method for the boltzmann equation on non-uniform grids, Journal of Computational Physics 227 (2008), no. 13, 6681 6695.
- 31. J.S. Hesthaven and T. Warburton, Nodal discontinuous galerkin methods: Algorithms, analysis, and applications, Texts in Applied Mathematics, Springer, 2007.
- 32. Ian Holloway, Aihua Wood, and Alexander Alekseenko, Acceleration of boltzmann collision integral calculation using machine learning, Mathematics 9 (2021), no. 12.
- 33. L. H. Holway, New statistical models for kinetic theory: methods of construction, Phys. Fluids 9 (1966), no. 9, 1658–1673.

- 34. Jingwei Hu, Jie Shen, and Yingwei Wang, A petrov-galerkin spectral method for the inelastic boltzmann equation using mapped chebyshev functions, Kinetic and Related Models 13 (2020), no. 4, 677–702.
- 35. I. Ibragimov and S. Rjasanow, Numerical solution of the boltzmann equation on the uniform grid, Computing 69 (2002), no. 2, 163–186.
- 36. Shashank Jaiswal, Alina A. Alexeenko, and Jingwei Hu, A discontinuous galerkin fast spectral method for the full boltzmann equation with general collision kernels, Journal of Computational Physics 378 (2019), 178 208.
- 37. Torsten Keßler and Sergej Rjasanow, Fully conservative spectral Galerkin-Petrov method for the inhomogeneous Boltzmann equation, Kinetic & Related Models 12 (2019), no. "1937-5093_2019_3_507", 507.
- 38. R. Kirsch and S. Rjasanow, A weak formulation of the Boltzmann equation based on the Fourier transform, Journal of Statistical Physics 129 (2007), no. 3, 483–492 (English).
- 39. Yu. Yu. Kloss, F. G. Tcheremissine, and P. V. Shuvalov, Solution of the Boltzmann equation for unsteady flows with shock waves in narrow channels, Computational Mathematics and Mathematical Physics **50** (2010), no. 6, 1093–1103 (English).
- 40. M.N. Kogan, Rarefied gas dynamics, Plenum Press, New York, USA, 1969.
- 41. Qin Lou, Xuhui Meng, and George Em Karniadakis, *Physics-informed neural networks for solving forward and inverse flow problems via the boltzmann-bgk formulation*, 2020.
- 42. Armando Majorana, A numerical model of the Boltzmann equation related to the discontinuous Galerkin method, Kinetic & Related Models 4 (2011), no. 1, 139–151.
- 43. A.B. Morris, P.L. Varghese, and D.B. Goldstein, *Monte carlo solution of the boltzmann equation via a discrete velocity model*, Journal of Computational Physics **230** (2011), no. 4, 1265 1280.
- 44. C. Mouhot and L. Pareschi, Fast algorithms for computing the Boltzmann collision operator, Mathematics of Computation **75** (2006), no. 256, pp. 1833–1852 (English).
- 45. Clément Mouhot and Lorenzo Pareschi, Fast methods for the Boltzmann collision integral., C. R., Math., Acad. Sci. Paris **339** (2004), no. 1, 71–76 (English).
- 46. Clément Mouhot, Lorenzo Pareschi, and Thomas Rey, Convolutive decomposition and fast summation methods for discrete-velocity approximations of the boltzmann equation, ESAIM: Mathematical Modelling and Numerical Analysis Modélisation Mathématique et Analyse Numérique 47 (2013), no. 5, 1515–1531 (eng).
- 47. Alessandro Munafò, Jeffrey R. Haack, Irene M. Gamba, and Thierry E. Magin, A spectral-Lagrangian Boltzmann solver for a multi-energy level gas, Journal of Computational Physics 264 (2014), 152–176.
- 48. A. Narayan and A. Klöckner, Deterministic numerical schemes for the Boltzmann equation, preprint.
- 49. V. A. Panferov and A. G. Heintz, A new consistent discrete-velocity model for the Boltzmann equation, Mathematical Methods in the Applied Sciences 25 (2002), no. 7, 571–593.
- 50. Lorenzo Pareschi and Benoit Perthame, A Fourier spectral method for homogeneous Boltzmann equations, Transport Theory and Statistical Physics 25 (1996), no. 3-5, 369–382.
- 51. Lorenzo Pareschi and Thomas Rey, Moment preserving fourier-galerkin spectral methods and application to the boltzmann equation, 2021.
- 52. F. G. Tcheremissine, Solution to the Boltzmann kinetic equation for high-speed flows, Computational Mathematics and Mathematical Physics 46 (2006), no. 2, 315–329.
- 53. _____, Method for solving the Boltzmann kinetic equation for polyatomic gases, Computational Mathematics and Mathematical Physics **52** (2012), no. 2, 252–268 (English).
- 54. J. Towns, T. Cockerill, M. Dahan, I. Foster, K. Gaither, A. Grimshaw, V. Hazlewood, S. Lathrop, D. Lifka, G. D. Peterson, R. Roskies, J. R. Scott, and N. Wilkins-Diehr, *Xsede: Accelerating scientific discovery*, Computing in Science & Engineering 16 (2014), no. 5, 62–74.
- 55. P. L. Varghese, Arbitrary post-collision velocities in a discrete velocity scheme for the Boltzmann equation, 25th International Symposium on Rarefied Gas Dynamics, 21–28 July 2006, Saint-Petersburg, Russia (Novosibirsk, Russia) (M.S. Ivanov and A.K. Rebrov, eds.), Publishing House of Siberian Branch of RAS, 2007, pp. 227–232.
- 56. Yanli Wang and Zhenning Cai, Approximation of the boltzmann collision operator based on hermite spectral method, Journal of Computational Physics 397 (2019), 108815.
- 57. Kyle Washabaugh, David Amsallem, Matthew Zahr, and Charbel Farhat, Nonlinear model reduction for cfd problems using local reduced-order bases.
- 58. L. Wu, C. White, T. J. Scanlon, J. M. Reese, and Y. Zhang, Deterministic numerical solutions of the Boltzmann equation using the fast spectral method, Journal of Computational Physics 250 (2013), 27 52.

- 59. L. Wu, J. Zhang, J. M. Reese, and Y. Zhang, A fast spectral method for the Boltzmann equation for monatomic gas mixtures, Journal of Computational Physics 298 (2015), 602 621.
- 60. Chenglong Zhang and Irene M. Gamba, A conservative discontinuous galerkin solver for the space homogeneous boltzmann equation for binary interactions, SIAM Journal on Numerical Analysis 56 (2018), no. 5, 3040–3070.
- 61. _____, A conservative discontinuous galerkin solver for the space homogeneous boltzmann equation for binary interactions, SIAM Journal on Numerical Analysis **56** (2018), no. 5, 3040–3070.

DEPARTMENT OF MATHEMATICS, CALIFORNIA STATE UNIVERSITY NORTHRIDGE, NORTHRIDGE, CA 91330, USA

Email address: alexander.alekseenko@csun.edu

Email address: robert.s.martin163.civ@army.mil

ARMY RESEARCH OFFICE, DEVCOM ARMY RESEARCH LABORATORY, DURHAM, NC 27709, USA

DEPARTMENT OF MATHEMATICS & STATISTICS, AIR FORCE INSTITUTE OF TECHNOLOGY, WPAFB, OH 45433, USA

Email address: aihua.wood@afit.edu